Theoretical study of tunneling phenomena in double-barrier quantum-well heterostructures

Gyungock Kim* and Gerald B. Arnold
Department of Physics, University of Notre Dame, Notre Dame, Indiana 46556
(Received 21 December 1987)

The resonant tunneling phenomenon through quantum-well states in one-dimensional double-barrier single-quantum-well heterostructures is studied with use of the nonequilibrium tunneling theory of Caroli *et al.* and a scattering-theoretic Green's-function technique with a simple model Hamiltonian. The effect of external bias is found exactly in the calculation of the Green's function for the junction within this model, obviating any restriction on the magnitude of the external bias. The density of states of the junction, its dependence on the external bias, and the formation of bound states in the quantum-well region are discussed. Our results for the tunneling current yield resonance peak-to-valley ratios in reasonably good agreement with experiment, indicating that this treatment of the tunnel junction, when applied to real materials, can more accurately describe existing experimental results.

I. INTRODUCTION

Chang, Tsu, and Esaki[1-3] first proposed and demonstrated resonant tunneling through quantum-well states and negative differential resistance in double-barrier $GaAs/Ga_{1-x}Al_xAs$ heterostructures. Since then, with the help of progress in molecular-beam-epitaxy growth techniques, there has been intensive concentration on these materials, both theoretically and experimentally.

Various experimental observations of electron and hole resonant tunneling in double-barrier single-quantum-well heterostructures, such as through ground and excited conduction states and quantized valence states of the quantum-well region, and the observation of resonant tunneling up to room temperature have suggested possible application to modern devices. It has been reported that the dc and high-frequency transport in these structures are important areas, especially the transport phenomena involving negative-differential resistance and multiple negative-differential resistance regions which can be employed in devices such as frequency multipliers, multistate memories, and the high-speed analog-to-digital converter.[4-11]

Most of the theoretical approaches in resonant tunneling through double-barrier heterostructures have been practically limited to the calculation of the transmission coefficient through the junctions. However, there exist some discrepancies between the conventional discussion and calculation of the transmission coefficient through the barrier and the experimental observations. One of the discrepancies between theory and the experimental observations is the resonant current peak-to-valley ratio in the current-voltage (I-V) characteristic curve. In the transmission-coefficient calculation, this value is usually very large compared to the experimental values. The reported observations of the resonant tunneling through confined excited states (valence and conduction bands) of the quantum well up to very high voltage cannot be predicted by effective-mass theory. The complicated features of hole resonant tunneling through heterostructures which are reported in Ref. 11 reflect the fact that the conventional calculational scheme of transmission coefficients does not accurately describe the tunneling phenomena in double-barrier heterostructures. Experiments find several negative-differential resistance regions up to very high voltage (around 2.3 V, which is about 4 times the barrier height in the experiment). This observation of unexpected negative-differential resistance in the high-voltage region cannot be explained in the conventional effective-mass theory. The report also suggests that the simple model of effective-mass theory is not good enough to describe the effect of the complicated valence-band characteristics on the formation of the bound state in the valence band of a quantum-well region, and that the effect of high voltage may cause considerable change in the electronic structure in a heterojunction.

Since one is dealing with atomic-scale, thin-layered structures in the tunneling experiments in heterojunctions, applied external voltage may alter the electronic structure in the thin films. Therefore a proper treatment of the effect of external potential is required in calculations of tunneling current through heterostructures. Explicit treatment of the external potential across the junction and its effect on the electronic structure of the heterojunction can improve the tunneling-current calculation, and can render the proper analysis for I-V characteristics of the tunneling through heterostructures.

Azbel *et al.*[12] obtained improvement in the calculation of the transmission coefficient of the junctions by considering the effect of the external field. In the calculation of transfer matrices[13] in their work, they consider the effect of voltage drop over the junction by introducing the WKB approximation, where a general form of the barrier potential and the potential drop in the quantum-well region are assumed. They reported that the resonant tunneling current is reduced by this consideration of voltage drop over the junction by 4 orders of magnitude in one example calculation. However, this approach is still semiclassical and is limited to a weak potential drop (smooth slope). Therefore this approach does not hold for the ultrathin-film case or high-voltage case. They also point out that the tunneling phenomenon is a time-

dependent process and might need explicit consideration of time factors which may be involved in the tunneling process.

In this paper we apply the previous nonequilibrium Green's-function technique by Caroli *et al.*[14,15] to tunneling in the double-barrier single-quantum-well heterostructures. The calculational scheme we use here is similar to the previous paper.[16] In this research we assume ideal junctions where we ignore any band bending or impurity-related effect. In the tunneling problem, one-dimensional aspects are prevailing factors. Since translational symmetry parallel to the interface planes is assumed for most of the tunneling problem in three-dimensional junctions, the problem is reduced to a quasi-one-dimensional problem. Therefore the layer representation simplifies the three-dimensional problem and reduces it to a quasi-one-dimensional problem. In this study we consider a one-dimensional two-orbital heterostructure model for simplicity. The extension of this technique to multiorbital three-dimensional problems is straightforward. We investigate the basic features of resonant tunneling using the nonequilibrium Green's-function technique, and the combination of electronic band structure with the tunneling-current formalism of Caroli *et al.* in the calculation of the resonant quantum-well tunneling. Although this model calculation study is not intended for any direct numerical quantitative comparison with specific existing experimental data, it suggests the qualitative features of resonant tunneling which were observed in experiments such as low-resonant-current peak-to-valley ratios, negative-differential resistance up to high voltages, and illustrates how the nonequilibrium technique for the tunneling current can predict the tunneling effect without considering time-dependent factors. This study also suggests possible applications to the calculations for real material heterojunctions. This formalism also gives a proper description for the high-voltage case and has advantages especially for very thin atomic-scale, layered junctions.

We organize this paper as follows. In Sec. II we present the model Hamiltonian and the calculational scheme of the Green's function for the one-dimensional double-barrier single-quantum-well heterostructure. In Sec. III the nonequilibrium Green's function and the tunneling-current expression are presented. In Secs. IV and V the local density of states of the heterojunction and the tunneling current through the quantum well are discussed.

II. HAMILTONIAN AND GREEN'S FUNCTION OF SEMICONDUCTOR HETEROJUNCTION

The Hamiltonian for a one-dimensional double-barrier heterosystem which is comprised of five subsystems, in terms of localized Wannier-like orbital basis functions $|b,n\rangle$, where b is an s or p orbital, and n is the one-dimensional layer index, is written as

$$H=\sum_{n}\sum_{b}E_b(n)\,|b,n\rangle\langle b,n| + \sum_{n,b}\sum_{n',b'}V_{bb'}(n,n')\,|b,n\rangle\langle b',n'|\ , \tag{1}$$

where $V_{bb'}(n,n')$ is the transfer integral and $E_b(n)$ is the local-site orbital energy. In Fig. 1, R and L indicate the right and left electrode, respectively, which may be either a metal or a doped semiconductor, regions 1 and 3 indicate the barrier regions (barrier 1 and barrier 2) which are semiconductors, and region 2 is the quantum well. Here we assume that the two barriers have N_1 and N_3 atomic layers, respectively, and the quantum-well subsystem is comprised of N_2 atomic layers. Four interfaces are formed between electrodes, barriers, and the quantum well in this heterosystem. At these interfaces, the transfer-integral matrices correspond to interfacial coupling matrices. The (2×2) interfacial coupling matrix defined between interface sites m and $m\pm1$ is

$$T(m,m\pm1)=V(n,n')\delta_{n,m}\delta_{n',m\pm1} = \begin{bmatrix} T_{ss}(m,m\pm1) & T_{sp}(m,m\pm1) \\ T_{ps}(m,m\pm1) & T_{pp}(m,m\pm1) \end{bmatrix} . \tag{2}$$

The first interface is formed between $n=0$ and 1, the second interface is located between $n=N_1$ and N_1+1, the third interface is formed between $n=N_1+N_2$ and N_1+N_2+1, and the fourth interface is between $N_1+N_2+N_3$ and $N_1+N_2+N_3+1$. For the middle quantum well a semiconductor or metal may be assumed

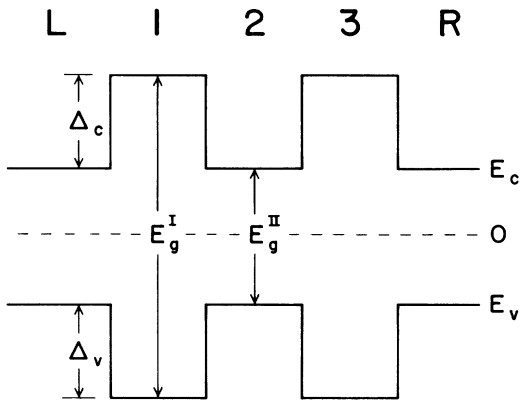

FIG. 1. Schematic energy diagram for a simplified one-dimensional double-barrier single-quantum-well heterojunction. L and R indicate the left- and right-electrode regions, respectively. Regions 1 and 3 indicate the barriers (barriers 1 and 2) and region 2 the quantum-well region. E_c (E_v) is the conduction- (valence-) band edge of bulk electrodes and quantum-well material. $E_g^{\rm I}$ is the bulk energy band gap of barrier 1 (barrier 2) and $E_g^{\rm II}$ is the energy band gap of the quantum-well (electrodes) bulk materials (superscripts I and II indicate regions 1 and 2, respectively). Δ_c is the conduction-band discontinuity and Δ_v is the valence-band discontinuity. Here, both of these parameters are defined from the bulk parameters (the energy band gaps of the bulk materials). We assume a symmetric band discontinuity for both valence and conduction bands for simplicity. Therefore the defined barrier height Δ is determined as the relative difference of the local-orbital energies between the barrier and the quantum well, that is, $\Delta=\Delta_c=\Delta_v=(E_g^{\rm I}-E_g^{\rm II})/2=E_p^{\rm I}-E_p^{\rm II}$. The actual effective barrier height of the thin quantum-size tunnel barrier depends on this parameter and the thickness of the barrier.

(Fig. 1 is drawn for the semiconductor case). The local density of states can be studied as a function of this interfacial coupling.[16,17] For the illustrative calculations in this paper, at each interface the interfacial coupling is taken to be equal to the geometric mean of the transfer integrals for the materials which form the interface. This choice is motivated by simplicity.

The approach in this research is that first we find Green's function for the isolated thin-film systems and then bring these five subsystems together by introducing coupling processes at the four interfaces, obtaining the Green's function of the whole junction.

In this semiconductor heterosystem, first, for the left and right electrodes two semi-infinite semiconductor subsystems are produced by removing the interaction between two adjacent sites from the perfect one-dimensional two-orbital crystal. This can be done by introducing perturbations which remove the intersite coupling in the Hamiltonian, so that a free surface is produced. In a similar way a thin semiconducting N-layer film can be produced by introducing the same perturbation N layers apart.[16-21]

The Hamiltonian H_0 for the perfect one-dimensional crystal in the Bloch basis is

$$H_0(k)=\begin{bmatrix} E_s+2V_s\cos(ka) & 2iV_{sp}\sin(ka) \\ -2iV_{sp}\sin(ka) & E_p+2V_p\cos(ka) \end{bmatrix} . \tag{3}$$

The retarded (advanced) Green's function $G_0^{r(a)}(k)$ is

$$G_0^{r(a)}(k)=1/[E\pm i\varepsilon-H_0(k)] , \tag{4}$$

where ε is an infinitesimal positive quantity. The Green's function in real space can be obtained as[18,21,22]

$$G_0^{r(a)}(n,n')=G_0^{r(a)}(n-n')=(1/2\pi)\int G_0^{r(a)}(k)\exp[ik(n-n')a]dk . \tag{5}$$

Therefore the retarded Green's matrix elements of the perfect one-dimensional crystal are as follows

$$\begin{aligned}
\langle s,n\mid G_0^r\mid s,0\rangle &= (4/h)[\alpha-\beta-(\alpha^2-1)^{1/2}+(\beta^2-1)^{1/2}]^{-1} \\
&\times\left[\frac{[\alpha(\alpha^2-1)^2]^{\mid n\mid}\{-V_p[\alpha-(\alpha^2-1)^{1/2}]^2+\zeta_p[\alpha-(\alpha^2-1)^{1/2}]-V_p\}}{[2(\alpha^2-1)^{1/2}][\beta-\alpha+(\alpha^2-1)^{1/2}+(\beta^2-1)^{1/2}]}\right. \\
&\left.-\frac{[\beta-(\beta^2-1)^{1/2}]^{\mid n\mid}\{-V_p[\beta-(\beta^2-1)^{1/2}]^2+\zeta_p[\beta-(\beta^2-1)^{1/2}]-V_p\}}{[2(\beta^2-1)^{1/2}][-\beta+\alpha+(\alpha^2-1)^{1/2}+(\beta^2-1)]}\right] , \\
\langle s,n\mid G_0^r\mid p,0\rangle &= (4V_{sp}/h)[\alpha-\beta-(\alpha^2-1)^{1/2}+(\beta^2-1)^{1/2}]^{-1} \\
&\times\left[\frac{[\alpha-(\alpha^2-1)^{1/2}]^{\mid n\mid}\{[\alpha-(\alpha^2-1)^{1/2}]^2-1\}}{[2(\alpha^2-1)^{1/2}][\beta-\alpha+(\alpha^2-1)^{1/2}+(\beta^2-1)^{1/2}]}\right. \\
&\left.-\frac{[\beta-(\beta^2-1)^{1/2}]^{\mid n\mid}\{[\beta-(\beta^2-1)^{1/2}]^2-1\}}{[2(\beta^2-1)^{1/2}][-\beta+\alpha+(\alpha^2-1)^{1/2}+(\beta^2-1)^{1/2}]}\right] \\
&=-\langle p,n\mid G_0^r\mid s,0\rangle , \\
\langle p,n\mid G_0^r\mid p,0\rangle &= (4/h)[\alpha-\beta-(\alpha^2-1)^{1/2}+(\beta^2-1)^{1/2}]^{-1} \\
&\times\left[\frac{[\alpha-(\alpha^2-1)^{1/2}]^{\mid n\mid}\{-V_s[\alpha-(\alpha^2-1)^{1/2}]^2+\zeta_s[\alpha-(\alpha^2-1)^{1/2}]-V_s\}}{[2(\alpha^2-1)^{1/2}][\beta-\alpha+(\alpha^2-1)^{1/2}+(\beta^2-1)^{1/2}]}\right. \\
&\left.-\frac{[\beta-(\beta^2-1)^{1/2}]^{\mid n\mid}\{-V_s[\beta-(\beta^2-1)^{1/2}]^2+\zeta_s[\beta-(\beta^2-1)^{1/2}]-V_s\}}{[2(\beta^2-1)^{1/2}][-\beta+\alpha+(\alpha^2-1)^{1/2}+(\beta^2-1)^{1/2}]}\right] .
\end{aligned} \tag{6}$$

Here,

$$\begin{aligned}
\alpha &= \mu+(\mu^2-\nu)^{1/2} , \\
\beta &= \mu-(\mu^2-\nu)^{1/2} , \\
\mu &= (1/h)(V_s\zeta_p+V_p\zeta_s) , \\
\nu &= (-4V_{sp}^2+\zeta_s\zeta_p)/h ,
\end{aligned} \tag{7}$$

where $h=4(V_sV_p+V_{sp}^2)$, $\zeta_s=\Omega-E_s$, $\zeta_p=\Omega-E_p$, and $\Omega=E+i\varepsilon$. Here, $(\alpha^2-1)^{1/2}$ is the square root whose imaginary part has the same sign as $\mathrm{Im}(\alpha)$. The same rule applies to $(\beta^2-1)^{1/2}$ and $\mathrm{Im}(\beta)$.

From now on we suppress retarded (r) or advanced (a) superscripts until explicit expressions are necessary. The Green's matrices G_R, G_L of semi-infinite crystals with perturbations $\mathbf{V}^R$ and $\mathbf{V}^L$ which produce right and left semi-infinite crystals and free surfaces satisfy the following Dyson's equations,

$$\begin{aligned}
G_R(n,n') &= G_0^R(n,n')+G_0^R(n,0)\mathbf{V}^R(0,1)G_R(1,n') \\
&= G_0^R(n,n')+G_0^R(n,0)[-V(0,1)]G_R(1,n') ,
\end{aligned} \tag{8a}$$

where $n,n'\geq 1$, and

$$\begin{aligned}
G_L(n,n') &= G_0^L(n,n')+G_0^L(n,1)\mathbf{V}^L(1,0)G_R(0,n') \\
&= G_0^L(n,n')+G_0^L(n,1)[-V(1,0)]G_L(0,n')
\end{aligned} \tag{8b}$$

for $n,n' \leq 0$. Here, G_0^R and G_0^L indicate the perfect-crystal Green's functions for right and left electrodes, respectively, and all matrices are 2×2 matrices.

The Green's function for three isolated thin films which will form two barriers and the quantum-well region later, where each region is comprised of N_1, N_3, and N_2 layers, respectively, are produced as follows. The perturbation $\mathbf{V}^\rho$ for each corresponding perfect crystal, where ρ indicates 1, 2, or 3, is defined as

$$\mathbf{V}^\rho=\sum_{b,b'}[-V^\rho_{bb'}(0,1)\,|\,b,0\rangle\langle b',1\,|\,-V^\rho_{bb'}(N_\rho+1,N_\rho)\,|\,b,N_\rho+1\rangle\langle b',N_\rho\,|\,]+\text{H.c.} \tag{9}$$

Here, H.c. means Hermitian conjugate. For each of these films, the Green's function satisfies the following equation,

$$G_\rho(n,n')=G_0^\rho(n,n')+G_0^\rho(n,0)[-V^\rho(0,1)]G_\rho(1,n')+G_0^\rho(n,N_\rho+1)[-V^\rho(N_\rho+1,N_\rho)]G_\rho(N_\rho,n')\ , \tag{10}$$

where $1\leq n,\ n'\leq N_\rho$, and G_0^ρ indicates the perfect-crystal Green's function for each region ρ. As mentioned in the previous work,[16] each isolated film has its quantized levels which show standing-wave-like characteristics and also depend on the thickness and energy band structure of the bulk crystal. A local perturbation can also be applied at the surface site to include the effect of a surface (or interface) which may be present in the heterostructure.

Isolated thin films and semi-infinite right and left electrodes are combined through the interfacial couplings to form a double-barrier structure. The coupling operator is defined as follows:

$$\begin{aligned}T=\sum_{b,b'}[&T^{\mathrm{I}}_{bb'}(0,1)\,|\,b,0\rangle\langle b',1\,|\,+T^{\mathrm{II}}_{bb'}(N_1,N_1+1)\,|\,b,N_1\rangle\langle b',N_1+1\,|\\&+T^{\mathrm{III}}_{bb'}(M,M+1)\,|\,b,M\rangle\langle b',M+1\,|\,+T^{\mathrm{IV}}_{bb'}(L,L+1)\,|\,b,L\rangle\langle b',L+1\,|\,]+\text{H.c.}\end{aligned} \tag{11}$$

Application of the external electric field leads to a potential drop across the junctions. We consider this external potential as a nonequilibrium perturbation and assume that the spatial variation of the external potential is confined to the double barriers and quantum-well region (semiconductor case). The external potential has the form of

$$\begin{aligned}&V^{\mathrm{ext}}=\sum_{n,b}V_b^{\mathrm{ext}}(n,n)\,|\,b,n\rangle\langle b,n\,|\ ,\\&V_b^{\mathrm{ext}}(n,n)=eV_0(L-n)/(L-1)\end{aligned} \tag{12}$$

where $L=N_1+N_2+N_3$.

For the left and right electrodes, there is a chemical-potential difference. This is the only effect of voltage on the electrodes. The Green's function G of the combined system and the Green's functions for three isolated thin films and semi-infinite electrodes satisfy the following recursive Dyson's equations in regions 1, 2, and 3 (Fig. 1) in the localized-orbital basis.

When $i,j\in$ region 1,

$$\begin{aligned}G(i,j)=&G_1(i,j)+G_1(i,1)T^{\mathrm{I}}(1,0)G(0,j)\\&+G_1(i,N_1)T^{\mathrm{II}}(N_1,N_1+1)G(N_1+1,j)\\&+\sum_{n\in\text{ region 1}}G_1(i,n)V^{\mathrm{ext}}(n,n)G(n,j)\ .\end{aligned} \tag{13}$$

If $i\in$ region 1, $j\notin$ region 1,

$$\begin{aligned}G(i,j)=&G_1(i,1)T^{\mathrm{I}}(1,0)G(0,j)\\&+G_1(i,N_1)T^{\mathrm{II}}(N_1,N_1+1)G(N_1+1,j)\\&+\sum_{n\in\text{ region 1}}G_1(i,n)V^{\mathrm{ext}}(n,n)G(n,j)\ .\end{aligned} \tag{14}$$

If $i,j\in$ region 2,

$$\begin{aligned}G(i,j)=&G_2(i,j)+G_2(i,N_1+1)T^{\mathrm{II}}(N_1+1,N_1)G(N_1,j)\\&+G_2(i,M)T^{\mathrm{III}}(M,M+1)G(M+1,j)\\&+\sum_{n\in\text{ region 2}}G_2(i,n)V^{\mathrm{ext}}(n,n)G(n,j)\ ,\end{aligned} \tag{15}$$

where $M=N_1+N_2$.

If $i\in$ region 2, $j\notin$ region 2,

$$\begin{aligned}G(i,j)=&G_2(i,N_1+1)T^{\mathrm{II}}(N_1+1,N_1)G(N_1,j)\\&+G_2(i,M)T^{\mathrm{III}}(M,M+1)G(M+1,j)\\&+\sum_{n\in\text{ region 2}}G_2(i,n)V^{\mathrm{ext}}(n,n)G(n,j)\ .\end{aligned} \tag{16}$$

If $i,j\in$ region 3,

$$\begin{aligned}G(i,j)=&G_3(i,j)+G_3(i,M+1)T^{\mathrm{III}}(M+1,M)G(M,j)\\&+G_3(i,L)T^{\mathrm{IV}}(L,L+1)G(L+1,j)\\&+\sum_{n\in\text{ region 3}}G_3(i,n)V^{\mathrm{ext}}(n,n)G(n,j)\ ,\end{aligned} \tag{17}$$

where $L=N_1+N_2+N_3$.

If $i\in$ region 3, $j\notin$ region 3,

$$\begin{aligned}G(i,j)=&G_3(i,M+1)T^{\mathrm{III}}(M+1,M)G(M,j)\\&+G_3(i,L)T^{\mathrm{IV}}(L,L+1)G(L+1,j)\\&+\sum_{n\in\text{ region 3}}G_3(i,n)V^{\mathrm{ext}}(n,n)G(n,j)\ .\end{aligned} \tag{18}$$

The Green's functions are found with the following relations:

$$\begin{aligned}&G(0,j)=G_L(0,0)T^{\mathrm{I}}(0,1)G(1,j)\ ,\\&G(L+1,j)=G_R(L+1,L+1)T^{\mathrm{IV}}(L+1,L)G(L,j)\ .\end{aligned} \tag{19}$$

All matrices are 2×2 matrices.

III. TUNNELING CURRENT

The tunneling current at the interface 1 assuming a stationary situation is

$$J_p=(e/ih)\sum_{l,l'}[T^{\mathrm{I}}_{ll'}(1,0)\langle c_l^\dagger(1,t)c_{l'}(0,t)\rangle - T^{\mathrm{I}}_{l'l}(0,1)\langle c_{l'}^\dagger(0,t)c_l(1,t)\rangle]$$
$$=(e/h)\int_{-\infty}^{\infty}\sum_{l,l'}[T^{\mathrm{I}}_{l'l}(0,1)G^+_{ll'}(1,0,E)-T^{\mathrm{I}}_{ll'}(1,0)G^+_{l'l}(0,1,E)]dE\ , \tag{20}$$

where l and l' are the orbital indices and $c_l^\dagger(1,t)$ and $c_l(1,t)$ are the creation and annihilation operators, respectively, for an electron in a localized state at site 1.

Nonequilibrium Green's functions $G^+(1,0)$, and $G^+(0,1)$ are

$$G^+(1,0)=G^+(1,1)T^{\mathrm{I}}(1,0)G^a_L(0,0)+G^r(1,1)T^{\mathrm{I}}(1,0)G^+_L(0,0)\ ,$$
$$G^+(0,1)=G^+_L(0,0)T^{\mathrm{I}}(0,1)G^a(1,1)+G^r_L(0,0)T^{\mathrm{I}}(0,1)G^+(1,1)\ , \tag{21}$$

where G^r_L and G^a_L are the equilibrium retarded and advanced Green's functions, respectively.

Since

$$H'=T+V^{\mathrm{ext}}\ , \tag{22}$$

$G^+(1,1)$ can be obtained from the following equation,

$$\langle b,1\,|\,G^+\,|\,b',1\rangle=\langle b,1\,|\,G^+_1\,|\,b',1\rangle+\sum_{n,n',l_1,l_2}\langle b,1\,|\,G^r\,|\,l_1,n\rangle\langle l_1,n\,|\,H'\,|\,l_2,n'\rangle\langle l_2,n'\,|\,G^+_1\,|\,b',1\rangle$$
$$+\sum_{n,n',l_1,l_2}\langle b,1\,|\,G^+_1\,|\,l_1,n\rangle\langle l_1,n\,|\,H'\,|\,l_2,n'\rangle\langle l_2,n'\,|\,G^a\,|\,b',1\rangle$$
$$+\sum_{n,n',n'',m}\sum_{l_1,l_2,l_3,l_4}\langle b,1\,|\,G^r\,|\,l_1,n\rangle\langle l_1,n\,|\,H'\,|\,l_2,n'\rangle$$
$$\times\langle l_2,n'\,|\,G^+_\rho\,|\,l_3,n''\rangle\langle l_3,n''\,|\,H'\,|\,l_4,m\rangle\langle l_4,m\,|\,G^a\,|\,b',1\rangle\ . \tag{23}$$

Here, b, b', l_1, l_2, l_3, and l_4 indicate s and p orbitals, and n, n', n'', and m indicate the layer indices. The index ρ of the equilibrium Green's function G^+_ρ indicates L, R, 1, 2, or 3 when both indices n' and n'' belong to the region L, R, 1, 2, or 3, respectively.

IV. DENSITY OF STATES IN A DOUBLE-BARRIER QUANTUM-WELL HETEROJUNCTION

It is known that an isolated thin film shows size-quantized levels which have standing-wave-like characteristics. When this thin film is coupled with the continuum states of semi-infinite electrodes in metal-semiconductor-metal junctions, and these states overlap in energies, the major feature in the local density of states of the semiconductor region is broadening of the quantized peaks. This broadening depends on the magnitudes of the interfacial couplings.

On the other hand, the local density of states of the double-barrier single-quantum-well heterostructure shows more complicated features. The local density of states of the whole junction can be studied as a function of the interfacial coupling perturbation. Since the continuum states in the electrodes and the quantized levels in the isolated thin films interact through the interfacial coupling perturbations, the quantized levels of the isolated thin films start to split, to have fine structure, and to be broadened as the coupling increases where the energies of the states overlap. The splittings and fine structure become smooth as the magnitude of interfacial coupling increases. As the interfacial coupling approaches the impedence-match limit,[17] the overall features of the local density of states of region 2 and the barriers are much smoother where they overlap in energy.

The formation of the quasibound states in the quantum-well region depends on several factors such as barrier and quantum-well thickness and electronic structure of materials which are used for barriers and region 2, the quantum-well region. When the formation of bound states is possible in the quantum-well region, the sharp quantized features still persist in the quantum-well energy range, where the densities of states in region 2 and the barriers do not overlap.

In this paper we study general qualitative features using a simple model. The parameters are chosen so that the conduction band is characterized mainly by p orbitals of atoms and the valence band mainly by s orbitals, and the parameter V_{sp} determines the mixing effect between s and p orbitals.[23–25] This model calculation is not intended for any numerical comparison with experimental data. However, we simulate the basic circumstances of tunneling through a heterojunction. We consider the conduction and valence-band characteristics by following the universal rule presented in Ref. 23, where the interatomic-orbital interaction parameters which determine the energy bandwidths are defined as $V_{ll'}=\eta_{ll'}\hbar^2/ma^2$. We choose a value for the interatomic p-orbital interaction $|V_{pp}|=\eta_{pp\sigma}\hbar^2/ma^2$, where $\eta_{pp\sigma}$ is

3.70 and the lattice constant a is around 4.3 Å. The same value for the interatomic s-orbital interaction is assumed for simplicity. The parameter V_{sp} is also used to change the curvature in the conduction and valence energy bands for fixed bandwidths. If the lower part of the conduction band participates in forming the eigenstate (actually in effective-mass theory, the effective-mass parameter m^* is determined by the curvature of the lowest conduction band at certain symmetry points), the energy range of interest in the conduction band in the semiconductor junction is of order of a few eV. We assume a finite width for the conduction band for convenience. This leads to consideration of the orbitals which participate in forming the eigenstates of the quantum well in real materials. The same values of $V_{ll'}$ are considered for both barriers, electrodes, quantum-well materials, and for interface-coupling matrix elements [impedance-matching values $T=(V^{\mathrm{I}}V^{\mathrm{II}})^{1/2}$ at interfaces are assumed] for simplicity. We also assume symmetric band discontinuities in both conduction and valence bands (i.e., $\Delta_c=\Delta_v=\Delta$) in the heterojunction for simplicity. (However, this assumption is not essential.) Therefore the barrier-height parameter Δ, which is a half of the difference of energy band gaps between bulk barrier and bulk quantum-well material here, is determined as the difference in local atomic-orbital energies of two materials, $E_p^{\mathrm{I}}-E_p^{\mathrm{II}}$. (However, this assumption is not essential and this formalism can be applied to any kind of heterojunction.) Since we assume a symmetric case for both conduction and valence bands, the same discussion holds for the resonant tunneling of holes through the valence-quantized level. The energy band gaps of both materials are assumed large enough (≥ 1.6 eV) that the tunneling of valence electrons through the conduction states of the quantum well and barrier, which may occur for a heterojunction with small energy gaps or with application of high external bias,[16] is negligible compared to the tunneling of conduction electrons in the considered range of external voltage. In an actual heterojunction, a slight complication might occur because of multiorbital features such as the multiorbital nature of the quantum-well bound eigenstates, and the structure factor due to basis atoms in the unit cell of a simple-cubic structure. These characteristics of the conduction and valence bands in the semiconductor depend on the details of real band structure. However, we expect that all the qualitative features discussed in this study will hold.

The positions and the widths of these quantized quantum-well levels are mainly determined by barrier height Δ, interfacial couplings, barrier and quantum-well thicknesses, and electronic structures of barriers and quantum-well materials for the ideal heterojunction. For instance, as barrier height increases or interfacial coupling decreases, the quantized level positions move upward in the quantum well. However, the level position is always lower than the isolated thin-film quantized levels in the conduction band of the quantum-well region in semiconductor heterojunctions. This is expected for the case of a particle in a quantum well with finite barrier height where the bound states in the well approach the quantized levels of the infinite well as barrier height Δ increases. The isolated thin film corresponds to the case of a particle in a well between infinitely high barriers ($\Delta\rightarrow\infty$).

In the following we illustrate the major changes of the quantum-well electronic states in various circumstances. The quantum-well quasibound states are rather sharply localized in the semiconductor quantum-well region. However, these electronic states have finite energy widths. When a few quantum-well states can be formed in the conduction band of the quantum-well region, the ground state has the narrowest energy width and the energy widths of the quantized quantum-well states are broadened as one goes higher in energy. In Fig. 2 we present an example of the local density of states $[D(n)=-\sum_b \mathrm{Im}G^r_{bb}(n,n)/\pi]$ at the interface site in the conduction quantum-well region which shows the dependence of the energy width of the quantized state on the barrier height Δ. From the left the barrier height Δ of each curve is 0.3, 0.4, and 0.5 eV and all of them have the same barrier thickness. The energy width of the peaks of bound states (near $E\approx 1$ eV) increases as the barrier height is decreased. Also note the change in peak positions. Even for the same barrier heights, as the barrier thickness increases the energy width of the quantized levels becomes narrower. The dependence of the energy width of the quantized levels on the barrier thickness is presented in Fig. 3. The barrier thickness increases

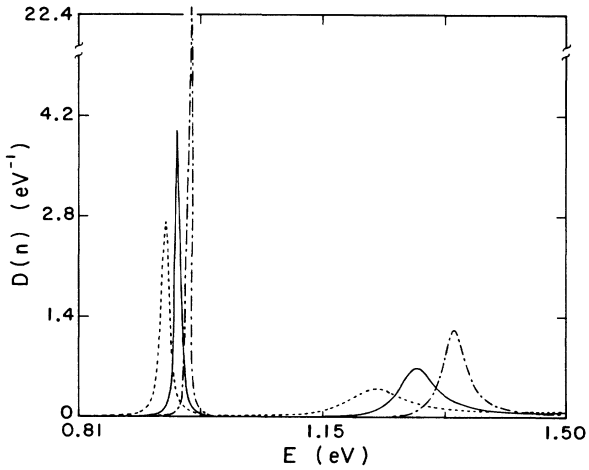

FIG. 2. Dependence of the local density of states in the conduction-band energy range at the interface site ($n=N_1+1$) of the quantum-well region on barrier height Δ for the symmetric heterojunction. The barrier height Δ is 0.3 (dotted curve), 0.4 (solid curve), and 0.5 eV (dashed-dotted curve). The local density of states has a sharp peak at the energy which corresponds to the quasibound states of the quantum well. (The first peak in each curve.) The continuum states of the junction start approximately from the second peak in each curve. Therefore these peaks indicate the effective barrier height of the junction (Ref. 16). The conduction-band edge E_c is 0.8 eV, that is, $E_g^{\mathrm{II}}=1.6$ eV. [Here, $-E_s^{\mathrm{I}}=E_p^{\mathrm{I}}=4.31$ eV, $-E_s^{\mathrm{II}}=E_p^{\mathrm{II}}=3.81$ eV, $V_s^{\mathrm{I}\,(\mathrm{II})}=T_{ss}^{\mathrm{I}\,(\mathrm{II,III,IV})}=1.5$ eV, $V_p^{\mathrm{I}\,(\mathrm{II})}=T_{pp}^{\mathrm{I}\,(\mathrm{II,III,IV})}=-1.51$ eV, and $V_{sp}^{\mathrm{I}\,(\mathrm{II})}=T_{sp}^{\mathrm{I}\,(\mathrm{II,III,IV})}=1.4$ eV for the dashed-dotted curve ($\Delta=0.5$ eV). The parameters E_b^{I} (subscript b is s or p) are adjusted accordingly to produce smaller Δ's. $N_1=N_2=N_3=10$ for all curves.]

through 5, 10, and 15 layers for the curves from the top. As is shown, the broadening of the quantum-well states increases with decreasing barrier thickness for fixed barrier height.

In each barrier region, unlike the single-barrier case, even at zero bias, an asymmetry in the density of states occurs across the barrier, because it is coupled to the continuum states of the electrode at one side and coupled to the thin-film quantized states at the other side. In the forbidden energy-gap range of the barriers, the local density of states has small peaked structure at the energies of the quasibound quantum-well states, which indicates the penetration of the quasibound states of the quantum well into the barrier region.

In the quantum-well region for the zero-bias case, if we assume the ideal situation where no impurities and surface perturbations cause asymmetry, a symmetry exists with respect to the line parallel to the interface, which bisects the middle of the quantum-well region. Therefore the density of states of the whole junction shows mirror symmetry with respect to the middle point of the quantum-well region. As an example, exactly the same shapes appear at the first and the last site in region 2 in the local density of states at zero bias as a result of the symmetric property in the local density of states throughout the junctions. The bound states in the quantum-well region have well defined peaks through the quantum-well region, and the local-density variations of the bound quantized levels in the well depend on the nodal and near-nodal behavior of the wave function.

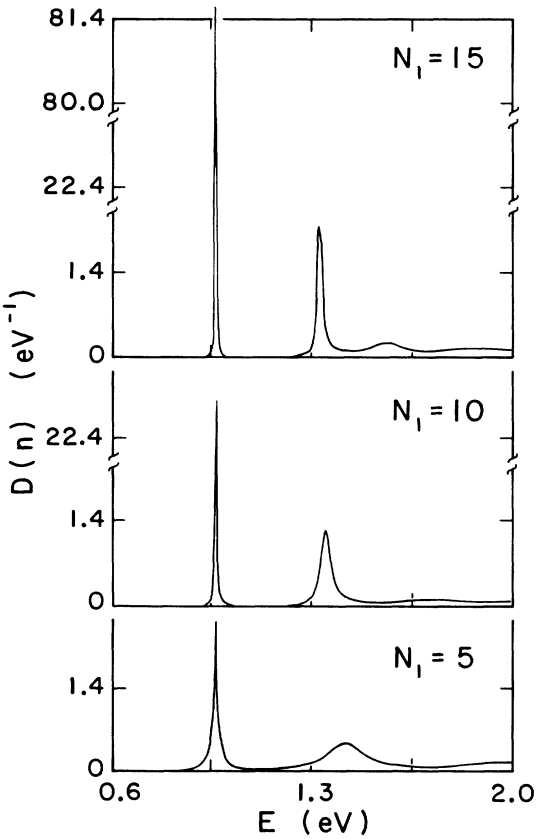

FIG. 3. The dependence of the quantum-well states on the barrier thickness ($N_1 = N_3$) for the symmetric heterojunction. As barrier thickness increases, the local density of states at the interface site in the quantum well ($n = N_1 + 1$) shows the quantized level with smaller energy width (more sharply localized bound state in the quantum-well region) which indicates a smaller probability for an electron to cross the barrier. Change in the thickness of the quantum-sized barrier influences not only the position of the quasibound quantum-well state, but also the effective barrier height in energy, which is, here, determined approximately by the position of the second peak in the density of states. [Here, the conduction-band edge $E_c = 0.8$ eV, the parameters are the same as the dashed-dotted curve ($\Delta = 0.5$) in Fig. 2, and $N_2 = 10$ for all curves.]

Application of the external voltage introduces asymmetry throughout the whole junction. As external voltage is increased the wave functions of quantum-well states are changed by the effect of the external bias. Therefore the symmetric property in the density of states with respect to the middle point no longer holds. As an example there is an asymmetry in the local density of states at the first and the last site at finite external bias. There exist broadenings of the peaks in the local density of states at finite bias, and the broadening in the peak of the local spectral density at the last site is greater than that at the first site in the quantum-well region. This is a natural consequence of the quantum-well quasibound state becoming closer to the continuum states of the right barrier in energy. The voltage-induced tilting effect on the local density of states of the whole junction in the presence of the external field contributes to the smaller peak-to-valley ratio in the I-V characteristics.

Not only V_{ll} (where l is s or p) but also V_{sp} in this model changes the curvature of the energy band. For a large value of V_{sp} in the quantum-well region, the energy-band curvature increases near the conduction-band minimum. This leads to the formation of the quasibound state at a higher energy. This is equivalent to the observation that a heavy-electron (-hole) quantum-well bound state is lower in energy than a light-electron (-hole) state in effective-mass theory. In Fig. 4(a) we present the average density of states per atom of each region in the conduction-band energy range at zero bias. In this case the value of V_{sp} is a half of that in Fig. 3. The density of states indicates a lower ground-state energy and also a higher-energy bound state in the quantum well (the second peak from the left) compared with Fig. 3. In Fig. 4(b) we present the average density of states per atom of each region of the junction which is subject to very high external bias, $V_0 = 1.4$ V, compared to the barrier height (around 3 times the barrier height) in the conduction-band energy range. The density of states of the junction shows rather complicated features in this high-external-bias case. In Fig. 4(b) the first two peaks in the spectral densities of states per atom in the quantum well, and the barrier-2 regions are derived from the two quasibound states at zero bias. However, the wave functions of these two states are quite different from those at zero bias. As is shown in the figures, if the external bias is increased up to a high value, the densities of states in the quantum well and in barrier 2 have additional peaks at the energy range below the continuum edge of barrier 1 (located near $E \approx 2.4$ eV), which belong to the smooth continuum

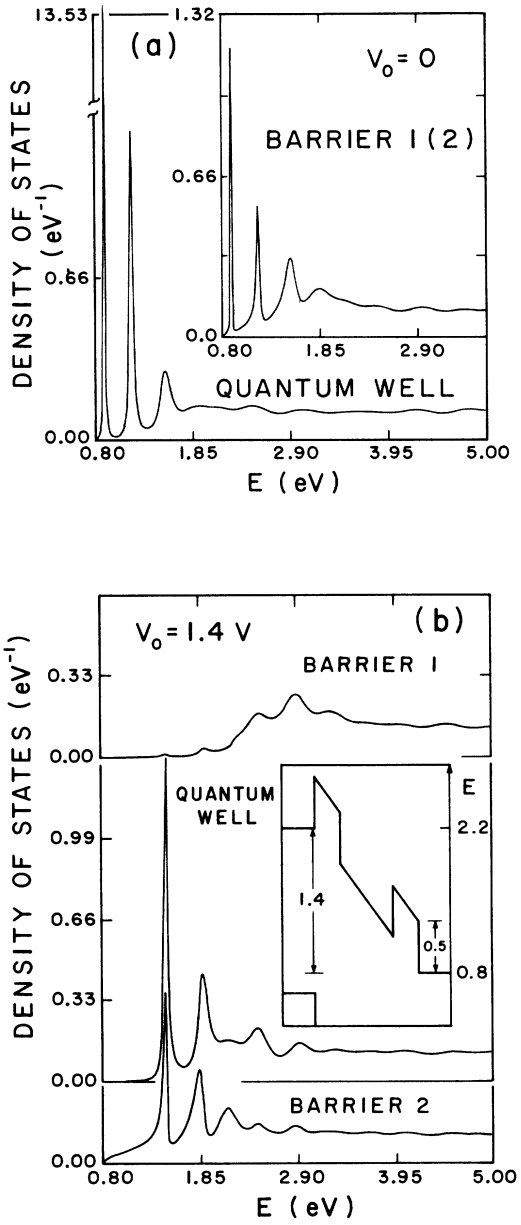

FIG. 4. The average densities of states per atom of quantum-well and barrier regions: (a) at zero bias and (b) at finite bias $V_0 = 1.4$ V. Here $V_{sp}^{I(II)} = T_{sp}^{I(II,III,IV)} = 0.7$ eV (half of that in Fig. 3), $E_c = 0.8$ eV, $\Delta = 0.5$ eV, $N_1 = N_3 = 5$, $N_2 = 10$, and the other parameters are as in Fig. 3. At zero bias, the density of states shows the quasibound quantum-well states in the quantum-well region, and the penetrations of these states into the barrier regions gives a finite amplitude in the densities of states of the barrier-1 and -2 regions. At $V_0 = 1.4$ V the first two peaks in the quantum well and barrier 2 originate from the quantum-well states at zero bias. However, as is shown in the density of states, the wave functions of these states are quite different from those of the zero-bias case due to the effect of high external bias. The third peak in the quantum well and barrier 2 indicates that the states are rather confined to the quantum-well and barrier-2 regions. The third peak, which is below the continuum edge of barrier 1 in energy, corresponds to the induced resonant state arising from the highly tilted junction potential due to the high external bias, as is shown in the schematic energy diagram.

states of the quantum well and barrier 2 at zero bias. These peaks can be clearly seen if we reduce the magnitude of the interfacial coupling matrix elements a little to see sharper features of these levels.[16] This state can be explained as the induced state due to the highly tilted potential in the junction, as is shown in the schematic diagram in Fig. 4(b). Therefore, these kinds of induced resonant states, which are rather confined in the quantum-well and barrier-2 regions, can give additional negative-differential resistance regions in the I-V curves up to the high external bias.

V. RESONANT TUNNELING

The nonequilibrium Green's-function approach for the calculation of the tunneling current in the tight-binding representation has advantages for atomic-scale layered heterojunctions where the quantum-size effects of the junctions are important, and where the spatial variation of the external potential over the interatomic distance in the junction is considerable. The effect of the external potential may alter the physical properties a great deal. For this reason, the effect of the external-potential perturbation is found to all orders in this research.

In Fig. 5 we present one example of I-V characteristics which shows the effect of the barrier height Δ on the tunneling current. The model junction in this figure corresponds to a 43 Å–43 Å–43 Å ($N_\rho = 10$, $\rho = 1$, 2, and 3) heterojunction. As in Fig. 2, the barrier height is changed through 0.3, 0.4, and 0.5 eV for the curves from the top, respectively, with fixed barrier and quantum-well thicknesses. The peak positions in current change as shown in Fig. 5(a). The calculated quantum-well state positions at zero bias are 0.09, 0.12, and 0.17 eV from the conduction-band edge E_c. The positions of peaks in current are at *about twice* the difference between these quantum-well bound levels and the equilibrium Fermi level. (Here the Fermi level is assumed to be 0.05 eV from the conduction-band edge E_c and the temperature is assumed to be 300 K.) The peak-to-valley ratio in the resonant tunneling current becomes smaller as the barrier height is decreased, which is shown clearly in Fig. 5(b), the natural-log–scale current-voltage [$(\ln I)$-V] graph. This indicates that the relative position of the peaks with respect to the barrier top plays an important role in determining the peak-to-valley ratio in resonant tunneling current. The resonant current peak-to-valley ratios are about 9:1 ($\Delta = 0.3$), 20:1 ($\Delta = 0.4$), and 45:1 ($\Delta = 0.5$). At low temperature (around 20 K) our calculated I-V curve for the same model junction with barrier height $\Delta = 0.3$ eV (which is not illustrated here) indicates a resonant peak-to-valley ratio of about 14:1. Although a direct comparison of this model calculation with experimental data is not intended in this work, we will mention experimental data to illustrate the qualitative improvement achieved in our calculation of the resonant current peak-to-valley ratio. In Ref. 4, for a $Ga_{1-x}Al_xAs/GaAs$ double-barrier single-quantum-well heterojunction (50 Å–50 Å–50 Å) with barrier height (Δ) 0.23 eV, the observed resonant peak-to-valley ratio in the tunneling current is 6:1 (4.8:1 at reverse bias) around 20 K (most of the other reported experimental results are smaller than

this, but, on the other hand, most of the conventional calculations of transmission coefficients yield values which are orders of magnitude larger). This indicates that the nonequilibrium treatment of the junction and explicit consideration of the external voltage yield reasonably better values for the resonant current peak-to-valley ratio and significantly improve the calculation of tunneling I-V characteristics in this type of heterojunction.

In Fig. 6 we present the dependence of tunneling current on the barrier thickness. The barrier height is fixed and the barrier thickness varies through 5, 7, 10, 12, and 15 layers for the curves from the top as in Fig. 3. Because the current varies over a wide range, the log-scale current-voltage graph is useful. As the barrier thickness increases, the quantum-well bound state is more localized in the quantum-well region. Therefore, as is shown in Fig. 3, the quantum-well quasibound state is more localized in energy (with smaller energy width) as the barrier thickness increases. This causes a larger peak-to-valley ratio in the tunneling current, as is shown in the natural-log–scale current and voltage curve. However, the peak-to-valley ratio is more moderate than is expected from the density of states at zero bias (at equilibrium). This shows that the effect of the external bias is partially to smooth the sharp features in the peak-to-valley ratio. Although the quasibound state at equilibrium (at zero bias) becomes more sharply localized in the quantum-well region for junctions as barrier thickness increases, the peak in the continuum region of the density of states for barriers (junction) moves closer to the quasibound-state energy as barrier thickness increases. The former effect sharpens the resonant current, and tends to increase the peak-to-valley ratio, but the latter effect decreases the effective barrier heights, tending to *decrease* this ratio. These two effects compensate to a certain degree. The magnitude of the peak of resonant current through the quantum-well state decreases exponentially as the barrier thickness increases, as expected.

The formation of the quantum-well bound states may also be influenced by local perturbations. The change in effective barrier height and width or local density of states at the interfaces due to local perturbations at interface sites in the barriers or in the electrodes or the quantum well affect the energy position of quantum-well bound states and tunneling current. The comparison among the cases with a local perturbation at interface sites in barriers (dashed-dotted curve), in the quantum well and the electrodes (dotted curve), and that without any local perturbations in the junction (solid curve) is presented in Fig. 7.

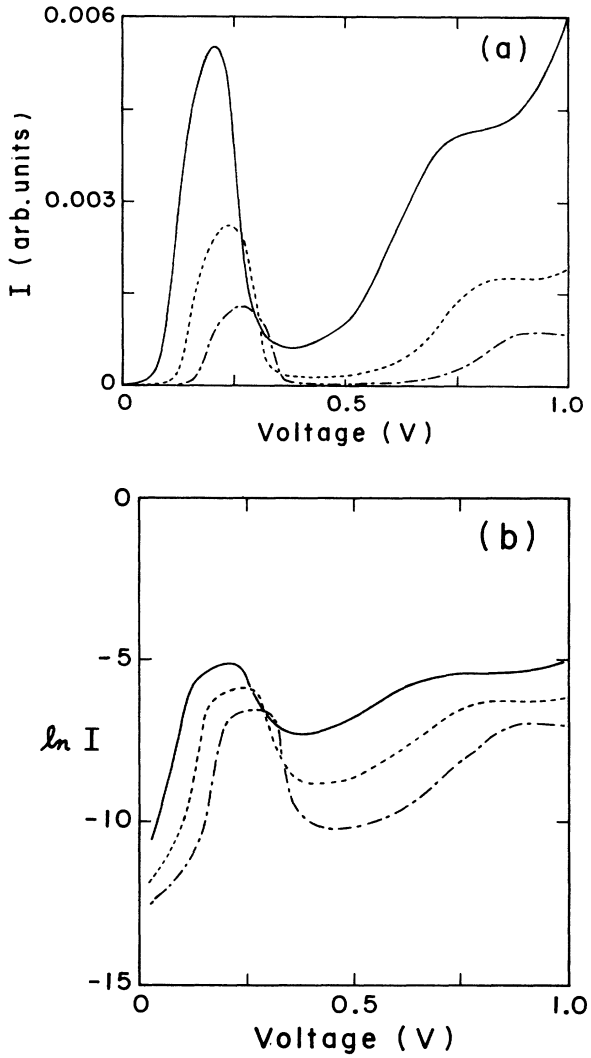

FIG. 5. The effect of barrier height Δ on the tunneling current (in units of $e/\hbar$). (a) The current-voltage (I-V) characteristic and (b) the ($\ln I$)-V for the heterojunctions with barrier height $\Delta=0.3$ (solid curve), 0.4 (dotted curve), and 0.5 eV (dashed-dotted curve). (Here, the temperature is assumed to be 300 K and the Fermi level from E_c is assumed to be 0.05 eV. Other parameters are the same as in Fig. 2.)

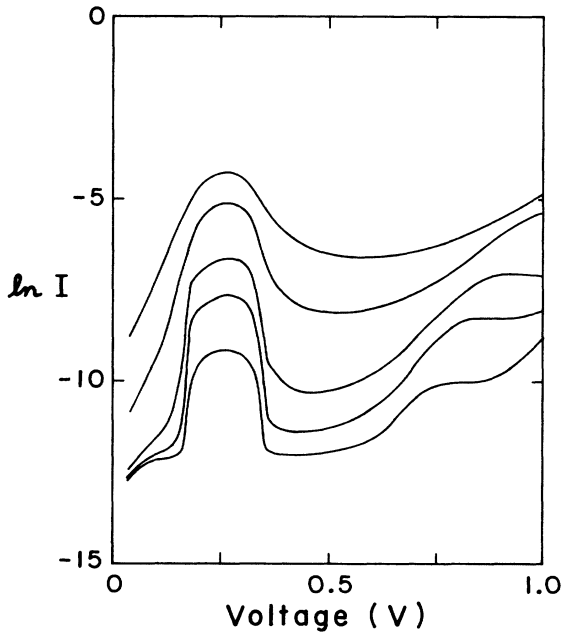

FIG. 6. The dependence of tunneling current (in units of $e/\hbar$) on the barrier thickness. $N_1=N_3=5$, 7, 10, 12, and 15 from the top, and $N_2=10$ for all curves. The same parameters as in Fig. 3 are used.

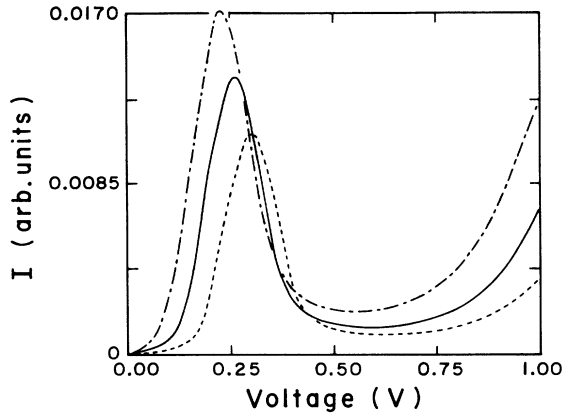

FIG. 7. The effect of the localized surface (or interface) perturbation on the tunneling current. The dashed-dotted curve is with local perturbations at the interface sites in the barriers ($U_{s\,(p)}^{\mathrm{I}\,(\mathrm{III})}=-0.2$ eV), the solid curve is without any local perturbation in the junction, and the dotted curve is with local perturbation at the interface sites in the quantum-well region and the electrodes ($U_{s\,(p)}^{L(R,\mathrm{II})}=0.2$ eV). ($N_1=N_3=5$, $N_2=10$, and other parameters are the same as in Fig. 3.)

The effect of heterojunction asymmetry on the tunneling current is presented in Fig. 8. Here the left barrier (region 1) is thinner than the right barrier (region 3). The solid curve corresponds to the reverse-bias case. The barrier asymmetry influences not only the resonant voltage but also the magnitude of the resonant tunneling current. As is shown in the figure, the different resonant voltages for each bias case reflect the thickness of each barrier of the junction. This barrier asymmetry of the junction induces a smaller magnitude of tunneling current in the reverse-bias case (when the thicker barrier is on the high-eV side).

In Fig. 9, two I-V curves are presented, where the value of V_{sp} for the dotted curve is half of that of V_{sp} for the solid curve. In the I-V curve with larger value of V_{sp} (solid curve), the first peak is due to the ordinary resonant tunneling through the quantum-well quasibound state.

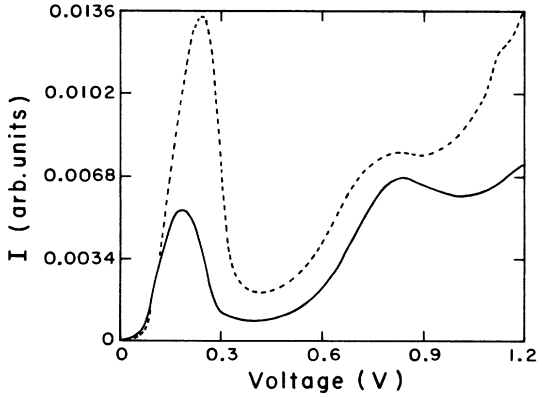

FIG. 8. The effect of geometrical asymmetry of barriers in the heterojunction for the dotted curve, $N_1=7$, $N_2=N_3=10$, $\Delta=0.3$ eV ($E_p^{\mathrm{I}}=4.11$ eV), and the other parameters are the same as in Fig. 2. The solid curve is the reverse-bias case.

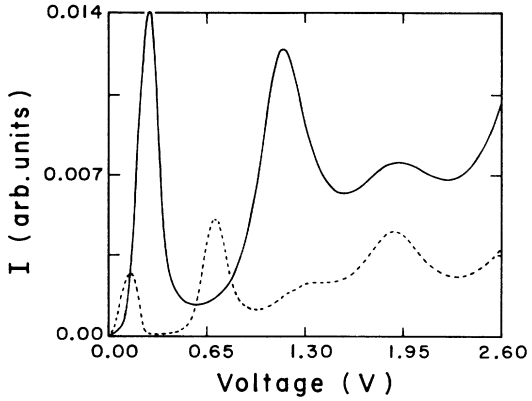

FIG. 9. Examples of tunneling current for a double-barrier heterojunction with different V_{sp} values. Here, V_{sp} is 1.4 (solid curve) and 0.7 (dotted curve). $N_1=N_3=5$, $N_2=10$, and the other parameters are the same as in Fig. 3.

The junction with the smaller value of V_{sp} (as is presented in Fig. 4) has a ground quasibound state at lower position in energy and an additional higher-energy bound state in the quantum well. These two states give the first and the second peaks in the dotted curve. In effective-mass–theory language, the larger V_{sp} value corresponds to a "lighter" electron than for the smaller V_{sp} value. Hence, it is not surprising to find a lower ground-state energy for the quantum-well quasibound state of the "heavy" electron (dashed curve) than for the "light" electron (solid curve). The other additional peaks and shoulders at higher voltages in the curves are due to resonant states which are induced because of the high applied external bias which produces an extreme tilting of band edges in the junction [as is illustrated in the schematic picture in Fig. 4(b)]. These resonances arise from above-barrier reflection processes which produce constructive interference between incident and reflected waves at certain energies. Therefore, as the external bias is increased, introduction of more resonant states becomes possible and these states can give additional negative-differential resistance regions in I-V characteristics. The potential contribution from the tunneling of valence electrons in the electrode, which is discussed in Ref. 16, is negligible compared to that of conduction electrons, even at the higher range of external bias (here 2.6 V), which is larger than the energy gap of the electrodes (here, $E_g^{\mathrm{II}}=1.6$ eV). (A similar argument holds for the case of hole tunneling.)

VI. SUMMARY

In this work the effect of external potential on a heterojunction is found exactly within a simple model, using a nonequilibrium approach. Several factors which influence the formation of the bound states in the quantum-well region are discussed. The effect of a thin quantum-size barrier is also considered explicitly. An improvement of the general features of I-V characteristics is obtained, so this presents a more realistic description for I-V characteristics than other models. Since the explicit electronic structure of the heterojunction is used in this

type of calculation, it is expected to produce more accurate results, and to predict the quantum-size effect more precisely than any other calculation. This formalism does not have any limitation on the magnitude of the external potential.

Our model calculation shows the major features that pertain to tunneling through a heterojunction. It also exhibits the general features which are expected in the conventional calculational scheme, while describing other features which are not obtained within the conventional scheme, but are observed, such as the negative-differential resistance at voltages far above the barrier height (Figs. 8 and 9). The success of this model calculation indicates that the use of realistic tight-binding band-structure parameters for real materials in the scheme presented here will be worthwhile.

---

*Present address: Howard Hughes Medical Institute, NSLS Bldg. 725-X4, Brookhaven National Laboratory, Upton, NY 11973.

[1]R. Tsu and L. Esaki, Appl. Phys. Lett. **22**, 562 (1973).

[2]L. Esaki and L. Chang, Phys. Rev. Lett. **33**, 495 (1974).

[3]L. Chang, L. Esaki, and R. Tsu, Appl. Phys. Lett. **24**, 593 (1974).

[4]T. Sollner, W. Goodhue, P. Tannenwald, C. Parker, and D. Peck, Appl. Phys. Lett. **43**, 588 (1983).

[5]S. Miyazaki, Y. Ihara, and M. Hirose, Phys. Rev. Lett. **59**, 125 (1987).

[6]M. Reed, J. Lee, and H. Tsai, Appl. Phys. Lett. **49**, (1986); M. Reed, Superlattices Microstruct. **2**, 65 (1986).

[7]S. Luryi, Appl. Phys. Lett. **47**, 490 (1985).

[8]J. Schulman and C. Anderson, Appl. Phys. Lett. **48**, 1684 (1985).

[9]T. Shewchuk, P. Chapin, and P. Coleman, Appl. Phys. Lett. **46**, 508 (1985).

[10]D. Roy, *Quantum Mechanical Tunneling and its Application* (World Scientific, Singapore, 1986).

[11]E. Mendez, W. Wang, B. Ricco, and L. Esaki, Appl. Phys. Lett. **47**, 415 (1985).

[12]B. Ricco and M. Azbel, Phys. Rev. B **29**, 1970 (1984).

[13]E. Bursetin and S. Lundquvist, *Tunneling Phenomena in Solids* (Plenum, New York, 1969).

[14]C. Caroli, R. Combescot, P. Noziéres, and D. Saint-James, J. Phys. C **4**, 916 (1971); R. Combescot, *ibid.* **4**, 2611 (1971); C. Caroli, R. Combescot, P. Noziéres, and D. Saint-James, J. Phys. C **5**, 21 (1972).

[15]L. Keldysh, Zh. Eksp. Teor. Fiz. **47**, 1515 (1964) [Sov. Phys.—JETP **20**, 1018 (1965)].

[16]G. Kim and G. B. Arnold (unpublished).

[17]M. Menon and G. Arnold, Phys. Rev. B **27**, 5508 (1983).

[18]D. Kalkstein and P. Soven, Surf. Sci. **26**, 85 (1971).

[19]J. Pollman and S. Pantelides, Phys. Rev. B **18**, 5524 (1978).

[20]A. Yaniv, Phys. Rev. B **17**, 3904 (1978).

[21]E. Foo and H. Wong, Phys. Rev. B **9**, 1857 (1974).

[22]E. N. Economou, *Green's Functions in Quantum Mechanics* (Springer-Verlag, Berlin, 1983).

[23]W. A. Harrison, *Electronic Structure and the Properties of Solids* (Freeman, San Francisco, 1980).

[24]G. A. Sai-Halasz, L. Esaki, and W. A. Harrison, Phys. Rev. B **18**, 2812 (1978).

[25]D. J. Chadi and M. L. Cohen, Phys. Status Solidi B **68**, 405 (1975).